Thermosetting Foam with a High Bio-Based Content from Acrylated Epoxidized Soybean Oil and Carbon Dioxide

Laetitia M. Bonnaillie, Richard P. Wool

Chemical Engineering Department, University of Delaware, Newark, Delaware 19716

Received 20 December 2005; accepted 18 December 2006
DOI 10.1002/app.26182
Published online 9 April 2007 in Wiley InterScience (www.interscience.wiley.com).

ABSTRACT: A resilient, thermosetting foam system with a bio-based content of 96 wt % (resulting in 81% of C_{14}) was successfully developed. We implemented a pressurized carbon dioxide foaming process that produces polymeric foams from acrylated epoxidized soybean oil (AESO). A study of the cell dynamics of uncured CO_2/AESO foams proved useful to optimize cure conditions. During collapse, the foam's bulk density increased linearly with time, and the cell size and cell density exhibited power-law degradation rates. Also, low temperature foaming and cure (i.e. high viscosity) are desirable to minimize foam cell degradation. The AESO was cured with a free-radical initiator (*tert*-butyl peroxy-2-ethyl hexanoate, $T_i \sim 60^\circ C$). Cobalt naphtenate was used as an accelerator to promote quick foam cure at lower temperature (40–50°C). The foam's density was controlled by the carbon dioxide pressure inside the reactor and by the vacuum applied during cure. The viscosity increased linearly during polymerization. The viscosity was proportional to the extent of reaction before gelation, and the cured foam's structure showed a dependence on the time of vacuum application. The average cell size increased and the cell density decreased with foam expansion at a low extent of cure; however, the foam expansion became limited and unhomogeneous with advanced reaction. When vacuum was applied at an intermediate viscosity, samples with densities ~ 0.25 g/cm^3 were obtained with small (<1 mm) homogeneous cells. The mechanical properties were promising, with a compressive strength of ~ 1 MPa and a compressive modulus of ~ 20 MPa. The new foams are biocompatible. © 2007 Wiley Periodicals, Inc. J Appl Polym Sci 105: 1042–1052, 2007

Key words: polymeric foam; bio-based; soybean oil; thermoset; cell structure

INTRODUCTION

Polymeric foams are complex structured gas–solid materials, consisting of a multitude of gas cells inside a solidified polymer matrix. This two-phase architecture presents numerous physical and mechanical advantages over bulk polymers, such as a higher weight-to-strength ratio, an added flexibility, lower thermal and electrical conductivities, as well as better shock absorption and sound-dampening properties.[1,2]

The U.S. foam market was estimated at more than 7.4 billion pounds in 2001 and is projected to grow nearly 3% annually to 8.5 billion pounds in 2006.[3] Densities of solid polymeric foams typically range from 0.016 to 0.960 g/cm^3, according to the needs of a wide range of applications that include furniture, construction, transportation (high density foams), cushioning, packaging (flexible foams), insulation, and filtration (low-density foams).[1,2] The principal raw materials currently used for the production of foam are petroleum and its derivatives. Since 1990, research has been active to incorporate plant-derived materials into existing polymeric systems and to create new bio-based polymers and polymeric foams.[4–23] The ideal replacement material would be renewable, offer comparable performance and price with petroleum-based foams, and be easily accessible to many countries in the world as well as optionally biodegradable. Plant-derived materials have the potential, both economically and environmentally, to fulfill these purposes. The most attractive candidate is the soybean, the world's largest source of vegetable oil [14]; the United States' production is abundant, with 600,000 soybean farmers producing more than 3 billion bushels soybeans in 2004.[24,25] The triglycerides constituting any plant oil can be chemically modified so as to become monomers or comonomers for several polymerization reactions.[14,15,18–20,22,26–31] Then, any polymer can theoretically be foamed.

Starch-based plastic foams[7,11,12,32–34] are used in specific industrial applications where biodegradability is required. Starch-based plastics are inexpensive, but water-sensitive. In 1999, the market for starch-based biopolymers was estimated at about

Correspondence to: L. M. Bonnaillie (bonnaill@che.udel.edu) or R. P. Wool (wool@ccm.udel.edu)

Contract grant sponsor: The National Research Initiative of the USDA Cooperative State Research, Education and Extension Service; contract grant number: 2005-35504-16137.

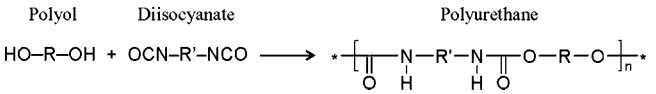

Figure 1 General polyurethane addition reaction.

20,000 t/a.[32] In 2002, the demand had grown to 23,000 t/a, with 75% used in packaging applications.[35]

Polyurethane (PU) foams are formed by reaction of a polyol with a diisocyanate, in 1 : 1 proportions of —OH and —NCO groups (Fig. 1), with the production of carbon dioxide gas from a side reaction with water.[36] Many different plant oil triglycerides—mostly soybean oil—have been successfully functionalized for the production of polyols used for PU plastics or foams; the triglycerides are first epoxidized with hydrogen peroxide and then the epoxy rings are opened with methanol.[13,37–40] In January 2004, the United Soybean Board estimated that 400 million pounds of soybean oil (Fig. 2) are used in synthesizing polyols for the production of PU foams.[25] Bio-based PU and PU foams display mechanical and thermal properties comparable with that of petroleum-based foams,[13] and soy-based polyols are cheaper than petroleum-based polyols.[25] However, because of the 1 : 1 stoechiometry of the polyol addition reaction with diisocyanate, the plant-based PU foams still contain a large fraction of petroleum-based material.

The *Affordable Composites from Renewable Resources* Group at the University of Delaware (ACRES) has designed several new thermosetting polymers from plant oils.[14,15,18–20,22,26–31] The present work uses one of the monomers studied by ACRES, acrylated epoxidized soybean oil (AESO), as shown in Figure 3. We designed a new foaming process inspired from the works of Wei and Mohamed on the foaming of polymer–fiber composites with pressurized nitrogen.[41,42] Our process uses carbon dioxide as a blowing agent to produce foams containing 96% plant-based material. Carbon dioxide is incorporated into the AESO monomer via diffusion and mechanical mixing at CO_2 pressures $\sim$ 60 bar and at room temperature. Then, the mixture is heated and foamed via pressure reduction. AESO is typically cured with a peroxide free-radical initiator.[14,22,43] We studied the rheology of AESO, the dynamics of uncured AESO/CO_2 foams, and added an accelerator to allow curing at lower temperature for a better foam stability. Examples of foams obtained are presented along with the dependence of foam structure on cure kinetics and some preliminary mechanical results. Projected applications include AESO/CO_2 foam cores for composite sandwich panels as designed by the ACRES Group for hurricane-resistant housing structures,[21,31,44,45] as well as windmill blades, sporting goods, tissue scaffold,[46] and all foam core composite applications.

EXPERIMENTAL

Materials

Monomer

Triglycerides are the main component of plant oils (Fig. 2). Soybean oil averages 4.2 double bonds per triglyceride. Figure 3 shows an AESO triglyceride. The details of the chemical reactions used to functionalize the triglycerides can be found in the works of the ACRES Group.[14,15,22,26,27] The C=C double bond in each acrylate group can react through a free-radical polymerization reaction using a peroxide initiator.

AESO was chosen for this study as it is the precursor of the line of bio-based polymers developed by the ACRES Group, and its mechanical properties can be controlled through the level of acrylation.[28] AESO, under the commercial name Ebecryl 860, was purchased from UCB Radcure. Each triglyceride of Ebecryl 860 possesses a statistical average of 3.4 acrylate groups.

During polymerization, AESO forms a rigid, thermosetting resin due to its high crosslinking potential; on average, 6.8 crosslinks per monomer can theoretically be created.[47] AESO and its derivatives have been found to exhibit tensile moduli in the range 1–10^3 MPa and glass transition temperatures in the range −50 to 150°C. Polymeric foams using AESO resins should prove strong enough to be used in structural applications, whether rigid or soft foams are required.

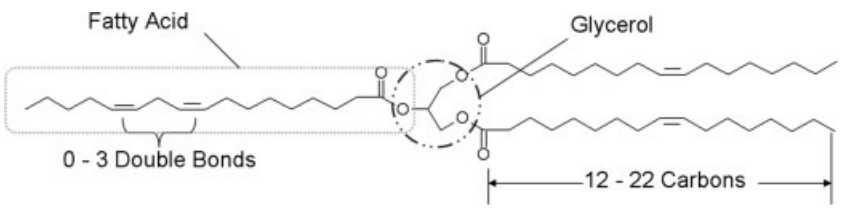

Figure 2 Structure of a triglyceride from plant oil. A glycerol center connects three fatty acids of variable length and number of insaturations.

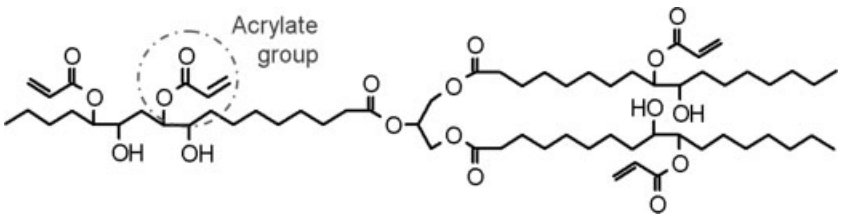

Figure 3 Acrylated epoxidized soybean oil monomer (AESO).

Blowing agent

Carbon dioxide was chosen as the blowing agent for many reasons: it is inexpensive, nontoxic, nonreactive, and environmentally benign. It is already used in polymer foaming processes as a replacement for HCFC gases[2] because of its high solubility in organic solvents ($\sim$ 2.5 mL/g at 25°C in benzene, toluene, or heptane, and even higher in methanol and acetone). Tanks of industrial-grade compressed CO_2 were purchased from Keen Compressed Gas.

Reagents

A peroxide, *tert*-butyl peroxy-2-ethyl hexanoate (Esperox 28, Witco), was used as free-radical initiator. It was chosen for its decomposition temperature (60°C). Cobalt Naphtenate with 6% metal content (CoNap, Witco) is used as an accelerator, allowing the free-radical initiator to decompose at temperatures lower than the initiation temperature of 60°C.

Sample preparation

Around 50 to 100 g of monomer was measured in a large glass beaker (600 mL or more). After the addition of 3 wt % of free-radical initiator, the mixture was stirred manually. Next, 1 wt % of accelerator was added and the mixture was vigorously stirred for homogenization. After stirring, some air stayed trapped in the mixture because of the high viscosity of AESO. The presence of air is undesirable as oxygen is a scavenger of free-radicals. The monomer mixture was air-purged, the sample was placed in a vacuum oven and submitted to maximum vacuum at room-temperature. The air/AESO foam was forced to rise under the pressure reduction (air bubbles growth followed the ideal gas law) and then collapsed because of excessive cell wall thinning at expansion ratios greater than 1000%. Next, the partially degassed sample was poured into a smaller glass liner (300 mL) that fits inside the base of the reactor. Vacuum was applied again and maintained until the air bubbling phenomena became negligible. The total purging procedure took about 1 h. The degassed sample was placed inside the reactor. A silicon O-ring and eight tightened bolts insured that the reactor's chamber was hermetically sealed to pressurized CO_2.

Foaming procedure

Figure 4 presents a schematic of the equipment used in this work. The 400-mL Parr high-pressure reactor containing the monomer sample was connected to a pressurized CO_2 tank. The entry valve was opened, and pressurized CO_2 was allowed to partially fill the reactor and then exit through a valve, in order to expel all air from the reactor (twice). Then, the exit valve was closed and the CO_2 pressure in the reactor was adjusted to $\sim$ 60 bar. The pressure in the reactor was measured with a manometer ($\pm$0.5 bar accuracy).

Pressurized CO_2 started diffusing into the monomer mixture at room temperature. The incorporation of CO_2 into the mixture was accelerated with mechanical stirring, in order to reach saturation quickly (30 min to 1 h was used). The amount of CO_2 dissolved determined the initial foam expansion and the ultimate foam density. The U-shaped stirrer was connected to a packed gland attached to an engine with a controlled rotation speed of $\sim$ 60 rpm.

While CO_2 was mixed with AESO, the external heater was brought to the chosen temperature T_H = 80–120°C. The heater was a 2-parts aluminum disc carved with a spiral-shaped channel for maximum residence time and heat-transfer efficiency. A silicon heating tape was wrapped around the metal then connected to a temperature controller. When the sampling valve was opened (at constant flow rate), the monomer–gas mixture rose inside the dipping tube, crossed the heater, and exited into a plastic mold at T_{foam} = 40–50°C and atmospheric pressure (P_{atm}). The sudden temperature increase from T_{room} to T_{foam} greatly accelerated the polymerization reaction, while the sudden pressure reduction triggered the formation of gas cells according to eq. (1):

$$\Delta P = \gamma / r \tag{1}$$

where ΔP is the difference between the pressure in the gas cell and the pressure in the liquid matrix, γ is the surface tension, and r is the gas cell's radius.[1]

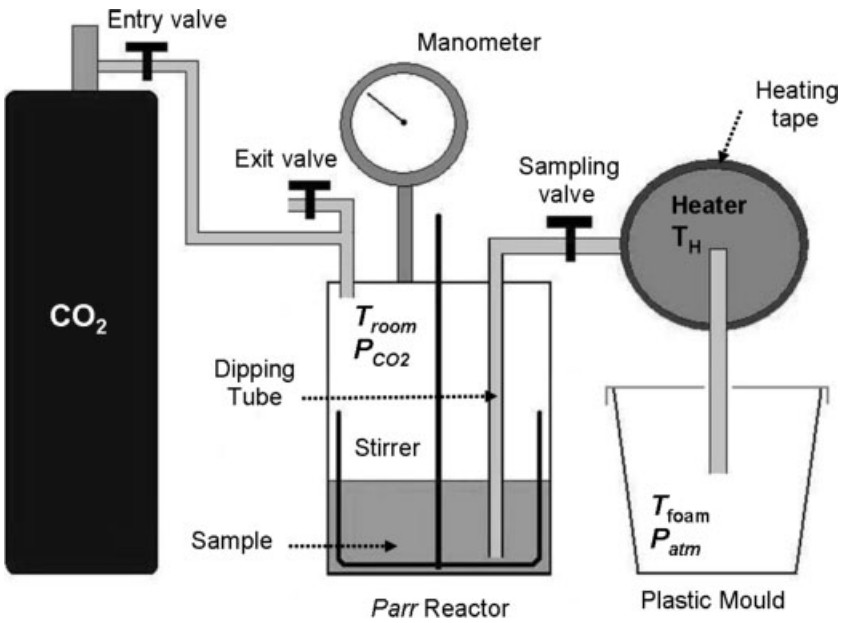

Figure 4 Simplified diagram of the low-temperature, pressurized carbon dioxide foaming process.

The foam density depends on the amount of CO_2 incorporated in the mixture during stirring. For additional foam expansion (i.e. lower density), the sample was placed in a vacuum oven and a partial vacuum was applied, before gelation, until the desired foam expansion was met. The possible expansion is limited by the extent of cure at the time of vacuum application and by the foam stability. In this work, densities of $\sim$ 0.25 g/cm^3 were successfully targeted.

The foam was kept at T_{foam} until a slight sample contraction was observed (unsticking from the mold's walls), that indicated solidification (gelation). Next, the foam was cured at a temperature T_2 slightly greater than T_i (e.g. 70°C) for several hours, to slowly decompose the rest of the initiator, then postcured at $T_3 = 100$°C for 2 h and $T_4 = 140$°C for 12 h.

All samples were cooled before characterization.

Foam characterization

Viscosity measurement

The viscosity of the liquid foam (precure) and of pure AESO were measured with a Brookfield viscometer, using the T-shaped spindles A (No. 91) or C (No. 93). Low rotation speeds were selected to minimize wrapping of curing material around the spindle. The spindle was located in the center of the sample, and viscosity was recorded as a function of time and/or temperature.

Bulk density

The foam's bulk density $\rho_{foam} = m_{foam}/V_{foam}$ was calculated as the ratio of the volume of the foam sample V_{foam} and its mass m_{foam}. For liquid foams, the volume was measured with a graduated cylinder ($\pm$0.2 mL accuracy). Solid foams were cut in parallelogram shapes and measured precisely in all three dimensions with a digital caliper. Weights were obtained with a precision scale ($\pm$0.0002 g accuracy).

Cell counting and measurement

While monitoring the variations of the bulk density of liquid AESO/CO_2 foams with time, we studied the growth of average foam cells. Fresh foam was poured in a transparent graduated cylinder, where gas cells can be observed on the wall. Pictures of the cylinder's wall were taken at different times, with a Canon Powershot S200 digital camera. Next, zooming on the central section of the cylinder, we selected a square area of fixed dimensions, where the number of gas cells in contact with the wall could be counted, as shown in Figure 5. For scaling, all dimensions on the picture were measured in pixels, then compared with the diameter of the cylinder (2.05 cm); e.g., on Figure 5 the cylinder's diameter was 1175 pixels; therefore the scale was 1175/2.05 = 573 pixels/cm (deformation because of the depth of the image was neglected). Each cell contained in a square of 200 $\times$ 200 pixels^2 was marked by a small dot (Fig. 6), then the cells were counted and the cell number as a function of time was recorded ($\pm$5% estimated accu-

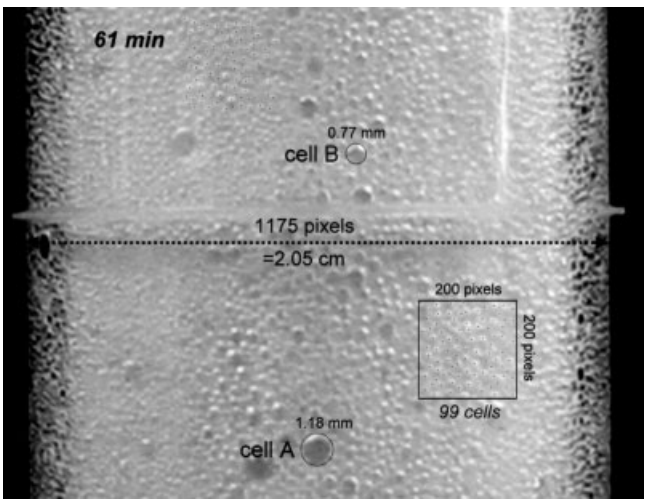

Figure 5 Digital picture of the central section of a foam inside a graduated cylinder, 61 min after pouring; the number of cells per unit area is counted to estimate the average cell size as a function of time. Two large cells A and B are highlighted for an observation of individual cell growth.

racy). The conversion from number of cells to average cells size is presented in the results section.

For the size measurement of an individual cell, we considered the cell to be spherical, and determined the diameter of the best fitting circle on the picture for that cell. See cells A and B in Figure 5.

Sample scans

To observe the cured foams' structure, samples were cut in half in the direction of foaming (i.e. vertically) using a precision hacksaw. The cut surfaces were then scanned with an Epson Perfection 1260 scanner at resolutions ranging from 600 to 2400 dpi depending on the desired visual precision. Picture dimensions were calculated from the scan's resolution. Scans were treated with PhotoImpact software.

Compression testing

Postcured foam samples were tested for compressive properties following the ASTM D1621 procedure. Parallelogram-shaped samples were polished with fine sand-paper (P320), and dimensions were measured with a micrometer. An Instron 4201 machine crushed the samples between two parallel metal plates at a rate of 2 mm/min. The load-deformation data were recorded by the Instron software, then converted to stress–strain curves using Microsoft Excel.

RESULTS AND DISCUSSION

Dynamics of liquid AESO foams

Liquid foams are subject to several destructive dynamics, including cell coalescence, cell coarsening, and rise and rupture of large cells at the foam's surface. These dynamics depend on the foam viscosity and the cells' size, which are a function of temperature, pressure, and time. In the next paragraph, we analyze some effects of these parameters on foam stability in order to optimize processing conditions.

Viscosity versus temperature

The viscosity of pure AESO was measured as a function of temperature. AESO was placed in a beaker and brought to 60°C with a heating plate. The viscosity was measured while cooling after removal of the heating plate. Figure 7 presents the viscosity profile of AESO as a function of temperature. The fitting of experimental data between 22 and 55°C shows that the viscosity obeys an Arrhenius law:

$$\eta_{AESO} = \eta_\infty \exp\left(\frac{E_\eta}{RT}\right) \text{ (in cp)} \qquad (2)$$

where η_∞ is the prefactor, and E_η is the activation energy for viscous flow. We found that for AESO,

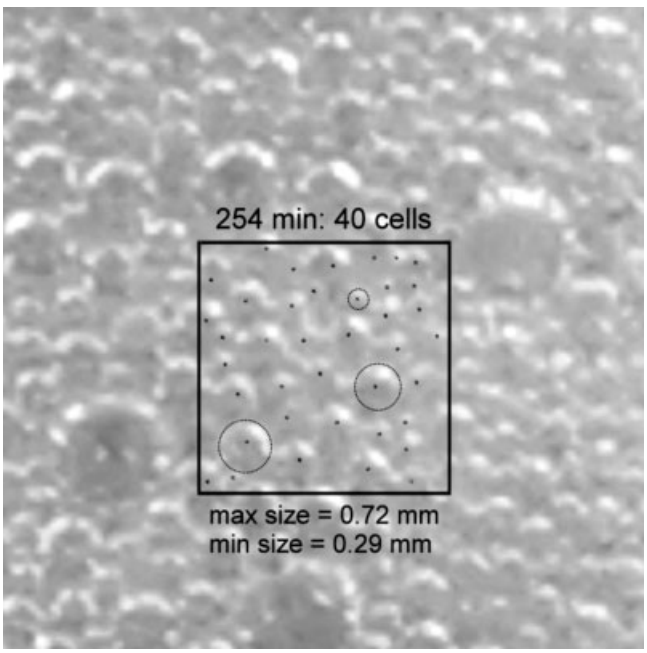

Figure 6 Cells are counted inside an area of dimension 200 pixel × 200 pixel. At $t = 254$ min, 40 cells are numbered (each cell is represented by a dot). Two large cells and a small cell are highlighted for an estimate of the size range.

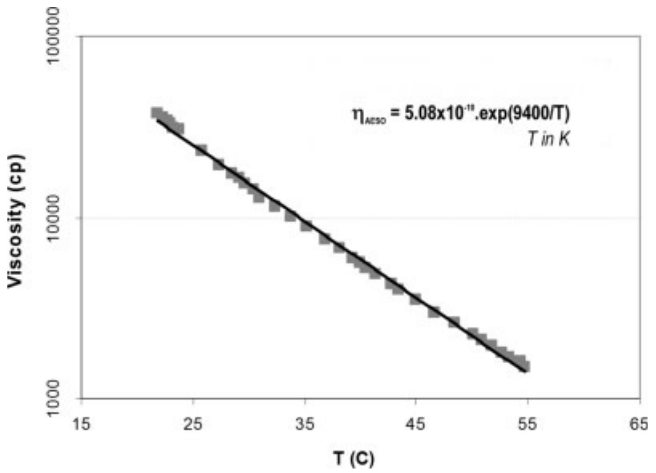

Figure 7 Viscosity (η) of ebecryl 860 (AESO) as a function of temperature during cooling. A Brookfield viscometer was used with the T-shaped spindle no. 93.

$\eta_\infty = 5.08 \times 10^{-10}$ cp, and E_η/R =9400 K. We can use this equation for extrapolation to temperatures below 22°C and above 55°C.

Liquid foams have a greater stability when the liquid's viscosity is high because of slower drainage of liquid from the cell walls and slower bubble rise. Temperature is critical regarding liquid foam stability: a temperature increase of only 5°C results in 43% viscosity reduction. Therefore, the lowest foaming temperature possible is to be chosen for the longest foam lifetime. At Esperox 28's initiation temperature of 60°C, AESO's viscosity is 27 times lower than at 25°C. For this reason, the CoNap accelerator was added to the system to allow polymerization at working temperatures lower than 60°C. Thus, samples we present in this work were cured at temperatures between 40 and 50°C.

Effect of time on bulk density

Our targeted cured foams have a low density (ρ ~ 0.25 g/mL) with small, homogeneous cells. However, the foam dynamics taking place before cure result in foam degradation via drainage, coalescence, and coarsening. Drainage of the polymer through gravity results in cell walls thinning. Coalescence involves the breakage of a wall between two cells to form one larger cell. Coarsening is caused by the pressure difference between a small cell and a large one [eq. (1)]; gas diffuses towards the region of lower pressure, the small cell disappears, and the large cell becomes larger. A combination of these three phenomena leads to a decrease in the number of cells, an increase in the average cell size, a reduction of the total foam volume from breakage of large cells at the top of the foam, and the ultimate total disappearance (collapse) of the foam.

AESO/CO_2 foam samples were poured into transparent Nalgene graduated cylinders, and kept at room temperature and atmospheric pressure. The external heater was not used and removed from the setup while pouring these samples. As degradation takes place, the sample's bulk density was recorded as a function of time. Figure 8 shows an example of bulk density as a function of time, where the foam was extracted from the reactor at $P_{CO_2} = 38$ bar and $T_{room} = 22$°C. The extracted foam is cold at first, due to vaporization of the dissolved CO_2, which is an endothermic phenomenon. When the foam temperature increases to room temperature, a slight expansion (i.e. density reduction) is observed. After maximum expansion, the sample's density begins to increase with time because of the rupture of cells at the surface. Large gas cells rise from the foam core and break on top of the sample. Figure 8 shows that after a short transition period (marked by t' ~ 50 min), the density increased linearly with time for the next 4 h. The linear region can be described as:

$$\rho(t) = \rho_0 + \alpha t \tag{3}$$

where $\rho_0 = 0.26$ g/mL and the slope $\alpha \sim 7 \times 10^{-4}$ g/(mL min).

Effect of time on cell size and cell density

The AESO/CO_2 foam was poured at room temperature ($T_H \sim 22$°C) into a transparent graduated cylinder. The cells on the wall of the cylinder were assumed to be representative of the cells in the core of the foam, and the cell size and cell density on the wall were followed as a function of time. Cells were counted as a function of time as described in the experimental section. For example, after 61 min

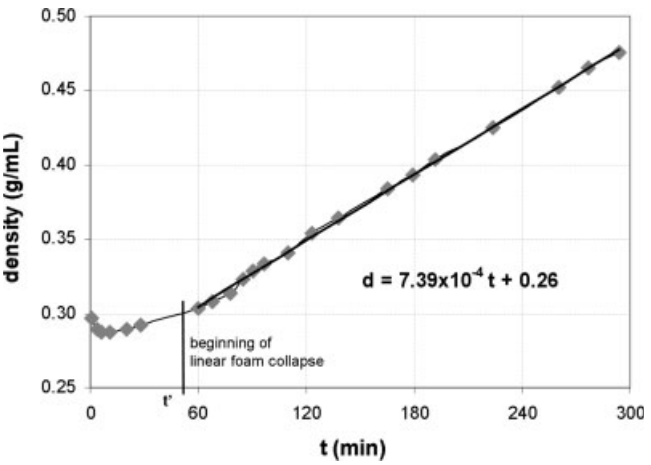

Figure 8 Foam density as a function of time for an AESO/CO_2 foam extracted from the high-pressure reactor at room temperature. $P_{CO_2} = 38$ bar and $T_{foam} = 22$°C.

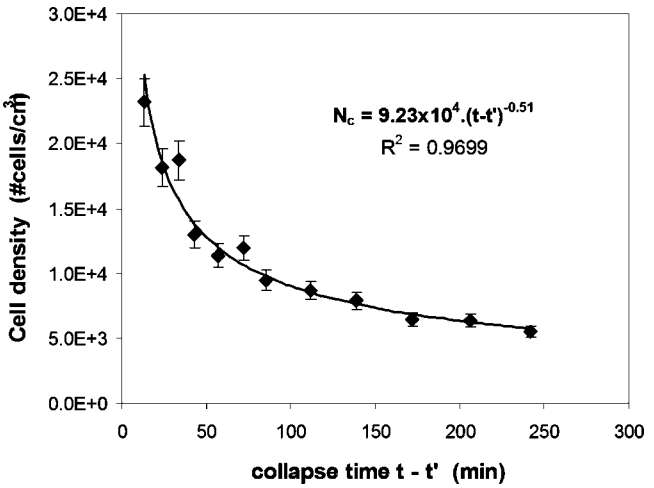

Figure 9 Volumetric cell density N_c as a function of time during linear foam collapse. The linear section of the foam collapse started at $t' = 48$ min.

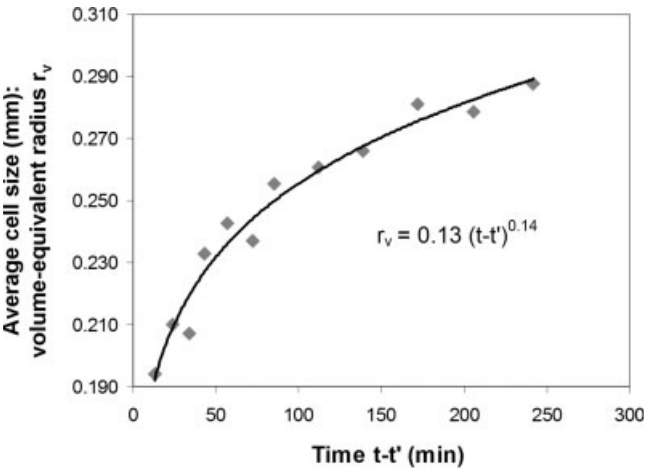

Figure 10 Volume-equivalent average cell radius r_V as a function of time during linear foam collapse.

we counted 99 cells (Fig. 5). After 254 min only 40 cells were left in an area of the same size (Fig. 6) because of coalescence and coarsening. The number of cells per unit area was then converted to the volumetric cell density N_c:

$$N_c = \left[\frac{\text{cell number}}{(200\ pixels)^2} \times \text{scale}^2\right]^{3/2} \quad (\text{in cells/cm}^3) \qquad (4)$$

The volumetric cell density as a function of time $N_c(t)$ is presented in Figure 9. N_c is seen to decrease proportionally to the inverse of the square root of time:

$$N_c \approx \frac{\alpha}{\sqrt{(t - t')}} \qquad (5)$$

where α is a constant and $(t - t')$ is the time elapsed since the beginning of linear foam collapse.

We then evaluated the average cell size as a function of time. The mean radius r_V of a cell was calculated from the following relation:

$$\frac{4}{3}\pi\, {r_V}^3 = \frac{V_{\text{gas}}}{N_c} \qquad (6)$$

where N_c is already known from eq. 4, and V_{gas} can be obtained from the foam density:

$$\rho_{\text{foam}} = \frac{m_{\text{AESO}}}{V_{\text{gas}} + \frac{m_{\text{AESO}}}{\rho_{\text{AESO}}}} \qquad (7)$$

The results for r_V (t) are presented in Figure 10. As expected, the average cell size increases with time. The cells' volume-equivalent radius appears to follow a power-law of the collapsing time: $r_V = 0.13\ (t - t')^{0.14}$.

Next, we followed the growth of two individual large cells: cell A and cell B from Figure 5. These cells are large enough to be visually measured by fitting their contour with a circle. Figure 11 features the bubble volume as a function of time for cell A and cell B. The two different growth mechanisms that coexist during foam collapse were observed:

1. Cell A grew almost linearly, owing to the slow diffusion of gas from smaller cells surrounding it (coarsening phenomena).
2. Cell B's linear growth was at some point rapidly accelerated and then it resumed. The sudden growth near 130 min was attributed to the fusion of cell B with a neighboring cell via

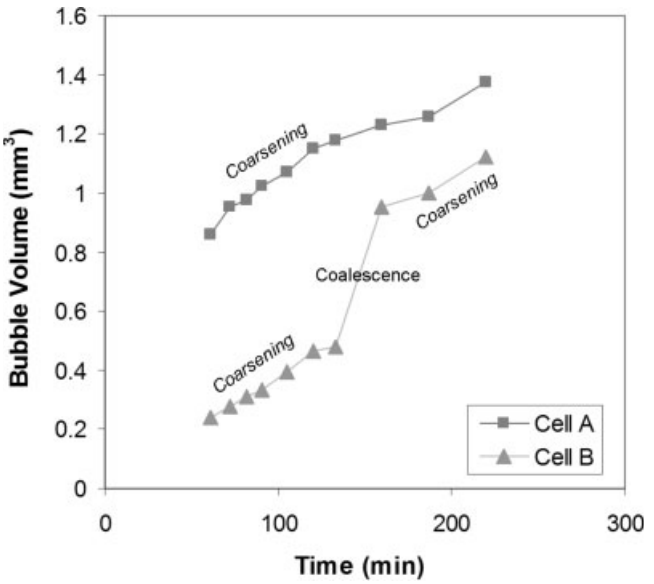

Figure 11 Growth of two large gas cells (cell A and cell B) during foam degradation as a function of time.

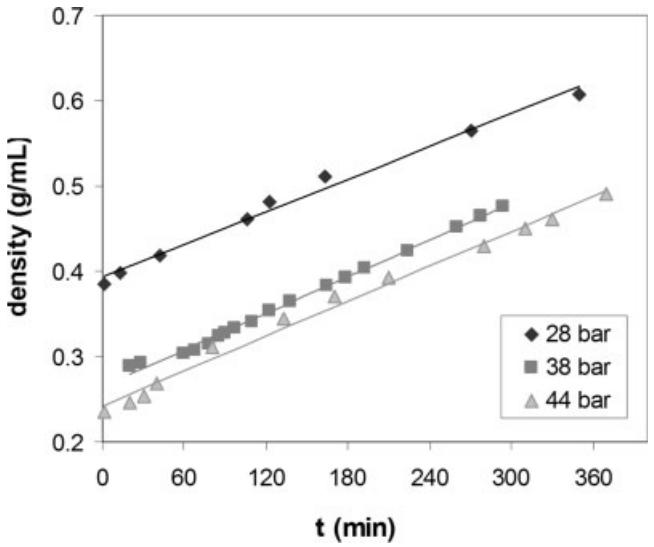

Figure 12 Collapsing rates of three AESO foam samples made from pressurization with CO_2 at P_{CO_2} = 28, 38, or 44 bar and T_{foam} =22°C.

coalescence. Observation of the series of pictures taken during foam collapse at cell B's location showed two neighboring cells at t = 130 min that became one cell at t = 160 min.

In consideration of these results, fast foam cure is necessary in order to keep the gas cells small and preserve a low foam density. The time limit for gelation can be obtained by reconciling the maximum cell size desired with the $r_V(t)$ profile of the corresponding sample foamed at P_{CO_2} and T_{foam}.

Effect of CO_2 pressure

Figure 12 presents the density profiles as a function of time for three AESO/CO_2 foam samples pressurized at P_{CO_2} = 28, 38, or 44 bars, then foamed at atmospheric pressure and allowed to collapse at room temperature. The initial foam density is seen to decrease with a higher CO_2 pressure. A higher CO_2 pressure resulted in a greater solubility of CO_2 in AESO. Therefore, a larger amount of gas dissolved and expanded at the time of foam extraction, producing foams with lower bulk densities. For foams with a low density, we should use the highest CO_2 pressure possible during the dissolution phase. In subsequent foam production, we always used the maximum CO_2 pressure allowed by the gas tank, i.e. $\sim$ 60 bar at 22°C. From Figure 12, we also noticed that there is no apparent influence of the initial foam density on the collapse rate. The slope of the three linear density profiles appears constant, with a collapse rate of $\sim 7 \times 10^{-4}$ g/(mL min). Therefore, in the density range considered, producing foams with a lower density does not decrease the foams' stability in a notable way.

Foam viscosity during cure

With insight from the liquid foam degradation dynamics, we chose to cure the foams at low temperature with the goal of obtaining gelation within minutes. When AESO was mixed with a thermal initiator only (e.g. Esperox 28) no cure was observed below the initiation temperature of 60°C. When the temperature was brought to above T_i, the cure was almost instantaneous. The introduction of cobalt naphtenate as an accelerator allows the initiator to decompose into two free-radicals at lower temperature, with the rate of decomposition increasing with increasing temperature.

Hong et al. showed that a 3 : 1 ratio of initiator/accelerator was efficient for room temperature cure within a few hours.[43] We found that at 25°C, sample thickening begins after $\sim$ 2 h, with a slow cure and progressive viscosity increase. In this study, we selected a cure temperature of 45°C to obtain a gelation time much shorter than 2 h and an initial viscosity four times higher than at T_i = 60°C.

The Rouse theory predicts that, up to the entanglement limit, the viscosity of a polymer is directly proportional to its molecular weight.[48] Therefore, the cure rate for AESO/Esperox 28 /CoNap/CO_2 foams was estimated through measurement of the viscosity as a function of time after extraction of the foam from the pressurized reactor. The heater temperature was set to 100°C in order to obtain a foam temperature of 45°C. The reactor pressure was set to P_{CO_2} = 58 bar (the maximum pressure allowed by the gas tank), resulting in foams with an initial bulk density of $\sim$ 0.42 g/cm^3. The time t = 0 indicates the beginning of foam extraction. Viscosity was recorded as a function of time until the polymer started climbing on the spindle's shaft, thereby preventing further accurate measurements. Figure 13 presents the viscosity profile as a function of time for a typical sample. We believe the initial delay observed was because of slow initiator decomposition kinetics and due to scavenging of the first free-radicals produced by the ambient oxygen and by an inhibitor (hydroquinone) premixed into Ebecryl 860. After $\sim$ 4.5 min, the foam's viscosity was seen to increase linearly with time for the next several minutes, which translates into a constant reaction rate. Finally, when polymer chains became long (after $\sim$ 6 min), they started wrapping and climbing on the shaft of the spindle, resulting in large oscillations in the viscosity measurement around an average value, with no further discernable viscosity increase. With a medium spindle rotation speed (20 rpm), the climbing phenomena started at $\eta \sim 2 \times 10^5$ cp. Reducing the

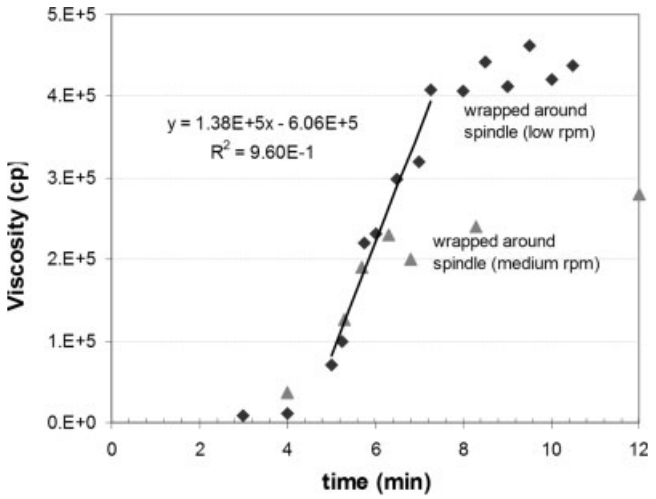

Figure 13 Viscosity profile of an AESO/CO_2 foam poured at $t = 0$ through the heater at $T_H = 100°C$. Isothermal cure with $T_{foam} = 45°C$. Viscosity measured with T-shaped spindle no. 91 at medium and low rotation speeds (20 and 4 rpm).

rotation speed to 4 rpm allowed monitoring the polymerization reaction up to a viscosity of $\sim 4 \times 10^5$ cp.

The results of this kinetic study were applied to the determination of satisfactory time for the application of vacuum after extraction of the foam, t_{vac}, and the correlation between the foam's structure and t_{vac}. Our goal was to trigger the cell growth via pressure reduction when the viscosity of the liquid phase was high enough to inhibit liquid drainage, coalescence and coarsening, and the crosslink density low enough to allow foam expansion. The following section presents cured foam samples that illustrate this principle.

Cured foam samples

All samples were a mixture of 96% AESO + 3% Esperox 28% + 1% CoNap (by weight) pressurized with CO_2 at 58 bar for 30 min and heated to 45°C through the external heater. The resulting initial foam density was ~ 0.42 g/cm^3. The samples were allowed to sit isothermally at $T = 45°C$ for different times t_{vac}, then submitted to −17.5 in.Hg vacuum at 45°C for 1/2 h or more. After this time, the samples were considered gelled and the postcure temperature sequence of 70, 100, and 140°C was applied, as described in the experimental section. Figure 14 and Table I present the results for three samples with $t_{vac} = 3$, 7, or 10 min, respectively. During vacuum application, the pressure reduction provoked instant cell growth according to eq. 1. The cells can be further enlarged with time via coalescence and coarsening, depending on the current liquid viscosity. These

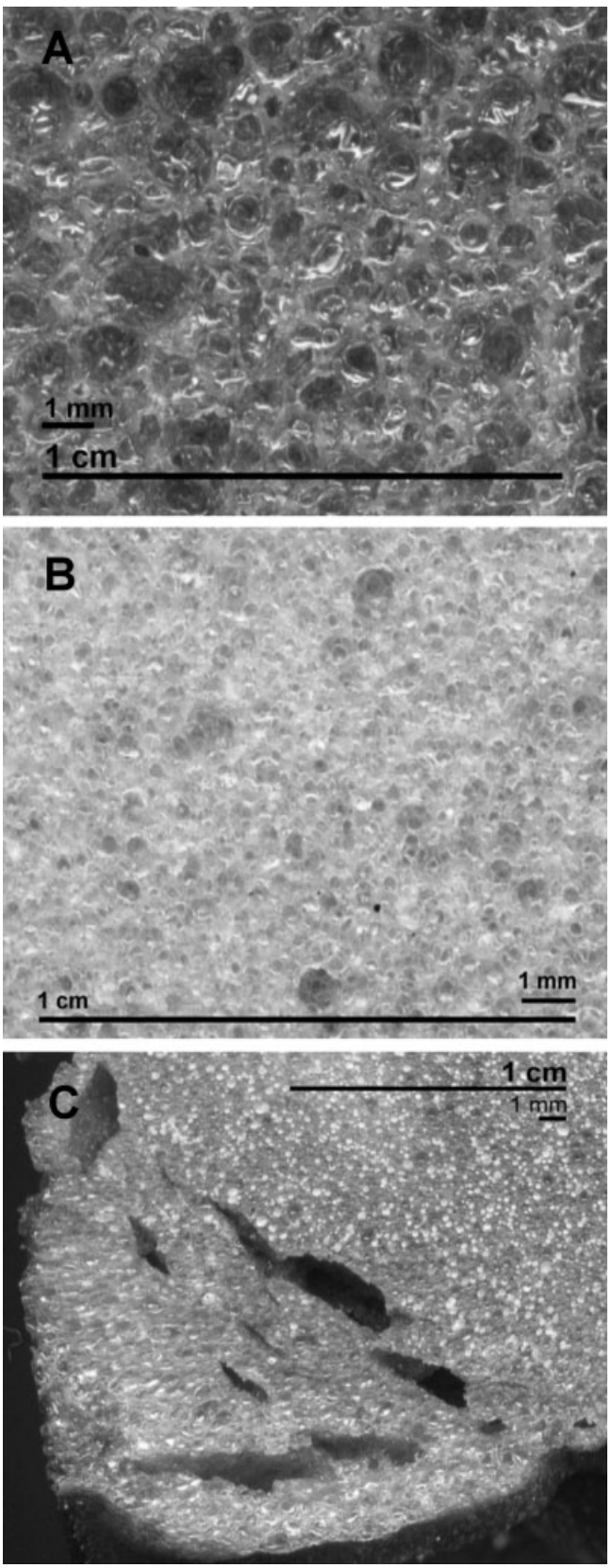

Figure 14 Scans of vertical cuts of three AESO/Esperox 28/CoNap/CO_2 foam samples foamed at $P_{CO_2} = 58$ bar and $T_{foam} = 45°C$, then submitted to −17.5 in. Hg vacuum after a time t_{vac}, then cured at 45°C and postcured. A: $t_{vac} = 3$ min, B: $t_{vac} = 7$ min, and C: $t_{vac} = 10$ min.

TABLE I
Cure Parameters, Foam Structure, and Compressive Properties for Three Samples Foamed at P_{CO_2} = 58 bar and T_{foam} = 45°C, then Submitted to −17.5 in.Hg Vacuum After a Time t_{vac}, and then Cured

Sample no.	T_{foam} (°C)	Time of vacuum application (t_{vac}; min)	Foam density (g/cm^3)	Cell size (mm)	Compressive strength (MPa)	Compressive modulus (MPa)
1	45	3 (premature)	0.23	0.2–2	~ 1.1	~ 23
2	45	7 (good)	0.23	0.1–0.3	~ 1.0	~ 18
3	45	10 (late)	0.48	0.05–0.2	N/A	N/A

two phenomena degrade the homogeneity of the foam. Sample 1 was expanded before the beginning of linear viscosity increase, i.e. before the cure had started (Fig. 13). The low viscosity existing at t_{vac} = 3 min allowed the reduction of the foam density to 0.23 g/cm^3, along with cell wall rupture and structural rearrangements, resulting in large cells of 1–2 mm diameter and a broad cell size distribution [Fig. 14(A)].

Sample 2 [Fig. 14(B)] was expanded 7 min after extraction. Referring to Figure 13, this time was just before the beginning of gelation, with a viscosity of almost 4×10^5 cp. The same foam density as with sample 1 was obtained. However, the small cells and good homogeneity of the foam on Figure 14(B) allow us to conclude that 4×10^5 cp is a better working viscosity for pressure reduction, low enough for easy foam expansion, and high enough to stabilize the individual cells.

Sample 3 [Fig. 14(C)] was expanded after 10 min, when the polymerization reaction was already advanced. Crosslinks had apparently begun to form, preventing foam expansion and keeping the cells small and the bulk density high (0.48 g/cm^3 once cured). The force applied by the pressure reduction created many cracks as well as small and large voids. Figure 14(C) features one of the bottom corners of the sample, showing small voids and a zone with larger cells where the polymer had a lower extent of cure due to contact with cold mold walls.

Mechanical properties

The compressive properties for samples 1 and 2 are given in Table I. The compressive strength was of the order of 1 MPa for both samples, and the compressive modulus was of the order of 20 MPa. Sample 3, with excessive structural flaws, was not tested. Industrial rigid foams typically display compressive strengths of ~ 1 MPa for densities of ~ 0.1 g/mL.

CONCLUSIONS

We developed a new lab-scale process for the production of polymeric foams from a thermosetting polymer and a pressurized gas. Applied to the AESO/carbon dioxide system, this process allowed the production of thermosetting foams with a high bio-based content. The ratio of $C_{14}/(C_{14} + C_{12})$ is 81%.

Room-temperature studies of liquid foam dynamics allowed the detailed observation of cell growth with time. It was noted than the sample's density increase is linear with time, and the slope does not depend on the initial foam density. The foam's structure (cell size and cell density) is seen to degrade rapidly with time; therefore foam samples must be cured quickly.

The lowest cure temperature (i.e. highest viscosity) is desired for the best liquid foam stability, precure. AESO/CO_2 foams were cured in less than 10 min at 45°C, using 3 wt % of Esperox 28 free-radical initiator coupled with 1 wt % of CoNap accelerator.

The cured foam's density was controlled by the application of a partial vacuum before gelation. Densities as low as 0.23 g/mL were obtained. The final structure of the foam proved highly dependent on the extent of cure at the time of vacuum application: the best structure (i.e. small, homogeneous cells) was obtained with expansion at high viscosity, i.e. just before gelation. After gelation, foam expansion was not possible anymore.

Mechanical properties comparable with those of semirigid industrial foams were obtained.

In future publications, we will study the improvement of the foam structure and mechanical properties through the use of additives and the optimization of process parameters.[49]

References

1. Klempner, D.; Frisch, K. C. Handbook of Polymeric Foams and Foam Technology; Oxford University Press: New York, 1991.
2. Landrock, A. H. Handbook of Plastic Foams: Types, Properties, Manufacture and Applications; Noyes Publications: New Jersey, 1995.
3. Rajan, M. U.S. Polymeric Foams Market to Cross 8.5 Billion Pounds by 2006. November, 30, 2001. Available from: http://www.bccresearch.com/editors/RP-120X.html.
4. Palsule, S.; Nema, S. K. Res Ind 1991, 36, 208.
5. Baser, S. A.; Khakhar, D. V. Cell Polym 1993, 12, 390.

6. Ge, J. J.; Sakai, K. Mokuzai Gakkaishi 1993, 39, 801.
7. Bhatnagar, S.; Hanna, M. A. Ind Crop Prod 1995, 4, 71.
8. Hatakeyama, H.; Hirose, S.; Hatakeyama, T.; Nakamura, K.; Kobashigawa, K.; Morohoshi, N. J Macromol Sci Pure Appl Chem 1995, 32, 743.
9. Ge, J. J.; Sakai, K. Mokuzai Gakkaishi, 1996, 42, 87.
10. Lin, Y.; Hsieh, F.; Huff, H. E. J Appl Polym Sci 1997, 65, 695.
11. Shogren, R. L.; Lawton, J. W.; Tiefenbacher, K. F.; Chen, L. J Appl Polym Sci 1998, 68, 2129.
12. Andersen, P. J.; Kumar, A.; Hodson, S. K. Mater Res Innovat 1999, 3, 2.
13. Guo, A.; Javni, I.; Petrovic, Z. J Appl Polym Sci 2000, 77, 467.
14. Khot, S. N.; Lascala, J. J.; Can, E.; Morye, S. S.; Williams, G. I.; Palmese, G. R.; Kusefoglu, S. H.; Wool, R. P. J Appl Polym Sci 2001, 82, 703.
15. Can, E.; Kusefoglu, S.; Wool, R. P. J Appl Polym Sci 2001, 81, 69.
16. Can, E.; Kusefoglu, S.; Wool, R. P. J Appl Polym Sci 2002, 83, 972.
17. Thielemans, W.; Can, E.; Morye, S. S.; Wool, R. P. J Appl Polym Sci 2002, 83, 323.
18. Bunker, S. P.; Wool, R. P. J Polym Sci Part A: Polym Chem 2002, 40, 451.
19. Wool, R. P.; Khot, S. N.; LaScala, J. J.; Bunker, S. P.; Lu, J.; Thielemans, W.; Can, E.; Morye, S. S.; Williams, G. I. In Advancing Sustainability through Green Chemistry and Engineering; Lankey R. L.; Anastas, P. T., Eds.; American Chemical Society: Washington, DC, 2002; pp 177–204.
20. Lu, J.; Hong, C. K.; Wool, R. P. J Polym Sci Part B: Polym Phys 2004, 42, 1441.
21. O'Donnell, A.; Dweib, M. A.; Wool, R. P. Compos Sci Technol 2004, 64, 1135.
22. LaScala, J. J.; Sands, J. M.; Orlicki, J. A.; Robinette, E. J.; Palmese, G. R. Polymer 2004, 45, 7729.
23. Wool, R. P. Chemtech 1999, 29, 44.
24. Good, D. Soybeans: Large Supplies Confirmed, But What About 2005 Production? Grain Price Outlook, January 2005, No. 2.
25. Soy-Based Thermoset Plastics, January 2004. Available from: http://unitedsoybean.org/f_media.htm.
26. La Scala, J.; Wool, R. P. J Am Oil Chem Soc 2002, 79, 373.
27. La Scala, J.; Wool, R. P. J Am Oil Chem Soc 2002, 79, 59.
28. La Scala, J.; Wool, R. P. Polymer 2005, 46, 61.
29. Lu, J.; Khot, S.; Wool, R. P. Polymer 2005, 46, 71.
30. Wool, R. P. (to University of Delaware, Newark, DE). U.S. Pat. 6,121,398 (2000).
31. Wool, R. P.; Sun, X. S. Biobased Polymers and Composites; Elsevier: Burlington, MA, 2005.
32. Bastioli, C. Starch/Starke 2001, 53, 351.
33. Fang, Q.; Hanna, M. A. Bioresource Technol, 2001, 78, 115.
34. Willett, J. L.; Shogren, R. L. Polymer 2002, 43, 5935.
35. Bioplastics, August, 2003. Available from: http://www.agr.gc.ca/misb/spec/index_e.php?s1=bio&page=plast2.
36. Woods, G. The ICI Polyurethanes Book. ICI Polyurethanes and Wiley: New York, 1990.
37. Petrovic, Z. S.; Guo, A.; Zhang, W. J Polym Sci Part A: Polym Chem 2000, 38, 4062.
38. Javni, I.; Petrovic, Z. S.; Guo, A.; Fuller, R. J Appl Polym Sci 2000, 77, 1723.
39. Zlatanic, A.; Lava, C.; Zhang, W.; Petrovic, Z. S. J Polym Sci Part B: Polym Phys 2004, 42, 809.
40. Petrovic, Z. S.; Guo, A.; Javni, I.; Zhang, W. Abstr Paper Am Chem Soc 2001, 222, U520.
41. Xu, W. Development and analysis of three-dimensionally reinforced cellular matrix composites, in Fiber and Polymer Science, North Carolina State University, Raleigh, NC, 2000.
42. Mohamed, T. S. Fabrication and analysis of three-dimensionally reinforced cellular matrix composites foamed by chemical blowing agent, in Textile Engineering, North Carolina State University, Raleigh, NC, 2002.
43. Hong, C. K.; Wool, R. P. J Appl Polym Sci 2005, 95, 1524.
44. Wool, R. P.; Khot, S. N.; LaScala, J. J.; Bunker, S. P.; Lu, J.; Thielemans, W.; Can, E.; Morye, S. S.; Williams, G. I. In Advancing Sustainability through Green Chemistry and Engineering; Lankey R. L., Anastas, P. T., Eds.; American Chemical Society: Washington, DC, 2002; pp 205–224.
45. Dweib, M. A.; Hu, B.; O'Donnell, A.; Shenton, H. W.; Wool, R. P. Compos Struct 2004, 63, 147.
46. Noack, C. L.; Zhu, L.; Bonnaillie, L. M.; Wool, R. P.; Klapperich, C. M. Biomaterials, submitted March 2007.
47. Khot, S. N. In Chemical Engineering; Ph.D. Dissertation, University of Delaware, Newark, DE: 2001.
48. Painter, P. C.; Coleman, M. C. Fundamentals of Polymer Science; Technomic: Lancaster, 1997.
49. Bonnaillie, L. M. In Chemical Engineering; Masters Thesis, University of Delaware, Newark, DE: 2004.